Electrochemically driven degradation of chemical solution deposited ferroelectric thin-films in humid ambient

Runar Plünnecke Dahl-Hansen, Jonathan Marc Polfus, Einar Vøllestad, Betul Akkopru-Akgun, Lyndsey Denis, Kathleen Coleman, Frode Tyholdt, Susan Trolier-McKinstry, and Thomas Tybell

View Online   Export Citation   CrossMark

ARTICLES YOU MAY BE INTERESTED IN

Electrochemically driven degradation of chemical solution deposited ferroelectric thin-films in humid ambient

Runar Plünnecke Dahl-Hansen,[1,2,3] (iD) Jonathan Marc Polfus,[2] (iD) Einar Vøllestad,[2] (iD) Betul Akkopru-Akgun,[4] (iD)
Lyndsey Denis,[4] (iD) Kathleen Coleman,[4] (iD) Frode Tyholdt,[3] (iD) Susan Trolier-McKinstry,[4] (iD) and Thomas Tybell[1,a] (iD)

AFFILIATIONS

[1]Department of Electronic Systems, NTNU—Norwegian University of Science and Engineering, 7491 Trondheim, Norway
[2]SINTEF Industry, Department of Sustainable Energy Technology, Forskningsveien 1, 0373, Oslo, Norway
[3]SINTEF Digital, MiNaLab, Gaustadaleen 23C, 0373, Oslo, Norway
[4]Department of Materials Science and Engineering and Materials Research Institute, The Pennsylvania State University,
University Park, Pennsylvania 16802, USA

[a]Author to whom correspondence should be addressed: thomas.tybell@ntnu.no

ABSTRACT

The ambient humidity significantly accelerates the degradation of lead zirconate titanate (PZT) films in microelectromechanical systems; the cause of such degradation is under debate. Here, it is shown that the degradation of chemical solution derived PZT thin-films in humid conditions is driven by the system's electrochemical activity toward water electrolysis. The layer stacks with Pt-based electrodes exhibited a faster degradation rate owing to their higher electrocatalytic activity compared to Au. A degradation model is proposed based on the electrolysis of liquid or gaseous H_2O, involving the evolution of oxygen and hydrogen gas at the top and bottom electrodes. Degradation proceeds above the threshold voltage for a given electrode system and is driven by the evolution and pressure build-up of gaseous species at the PZT/electrode interfaces. The pressure build-up causes film cracking, delamination of the film and electrodes, electrothermal breakdown events, and eventually time-dependent dielectric breakdown. Significantly larger post-breakdown crater sizes in humid than in dry conditions suggests that larger cracks through which dielectric breakdown through humidified air can occur. Overall, these effects are shown to cause sample failure up to six orders of magnitude of time earlier than for operation in dry conditions. Thus, in order to improve the resilience of thin-film systems in humid conditions, it is imperative to protect the electrochemically active electrode components of the device.

Published under license by AIP Publishing. https://doi.org/10.1063/5.0003989

I. INTRODUCTION

Lead zirconate titanate (PZT) films are utilized in piezoelectric microelectromechanical system (piezoMEMS) applications due to their large dielectric and piezoelectric compliances.[1,2] For thin-film piezoMEMS operating under high electrical fields, improving the films' electromechanical reliability is key for widespread adaption.[3,4] The electrical and electromechanical properties of PZT-based thin-film piezoMEMS are generally known to be heavily influenced by the humidity-level of the operating ambient.[5–7] In dry conditions, electrical degradation stems from a field-dependent combination of Schottky and Poole-emissions.[8–12] The associated barrier heights and activation energies are strongly affected by the film/electrode

interface, the film defect chemistry,[13–18] and the work function of the electrode systems.[10] Over time, the accumulation of oxygen vacancies at the cathode interface will increase charge injection and cause time-dependent dielectric breakdown (TDDB).[15,16] Well-processed single- and polycrystalline films, however, show typical lifetimes, suggesting that the piezoelectric device should be able to survive for realistic product lifetimes in dry operating conditions.[16]

In humid conditions, TDDB typically occurs through the early onset of leakage transients and electrothermal breakdown events (ETB), significantly faster than in dry conditions.[19] Different mechanisms may govern such humidity-induced breakdown depending on the layer stack of the piezoMEMS-devices. Humidity can, for

example, catalyze electromigration of Ag or Ni electrodes, resulting in the growth of conductive metal filaments from the anode, through the thin-film to the cathode. Such mechanisms eventually cause leakage transients, ETB, and TDDB.[20–23] On the other hand, recent reports suggest that the electrolysis of water may be key to understanding the mechanisms governing humidity-induced degradation.[24–34] This may be particularly important for commonly used electrode systems for piezoMEMS-devices, such as Pt,[12] SrRuO$_3$,[35] or IrO$_2$,[36] displaying generally high electrochemical activity.[24] During water electrolysis, the anodic oxidation of water produces protons that can drift from the anode to the cathode, forming an electrolytic cell.[37] Protonic defects dissolved interstitially in PZT by the hydration of oxygen vacancies[38] can impede the cubic-tetragonal phase transition,[39] change the film's polarizability,[40] reduce the optical band gap,[41] decreases fracture toughness,[42,43] and/or cause severe resistance degradation.[44] However, such effects have primarily been measured after exposure to elevated temperatures during film-processing. Thus, for thin-film PZT-based piezoMEMS, it is still debated which effect is driving the highly accelerated TDDB in humid operating conditions.[21,22,26,45,46]

If, in fact, water electrolysis governs breakdown in humid environments, alternative approaches for studying the degradation should be investigated. Here, it is shown that in humid and wet conditions, the degradation of PZT thin-films deposited by chemical solution-deposition (CSD) is driven by the electrochemical activity of the layer-stack. A degradation model is proposed based on the formation and transport of protonic charge carriers from the electrolysis of water. Degradation proceeds above a threshold voltage for a given electrode system and is driven by the evolution and pressure build-up of oxygen and hydrogen gases at the PZT/electrode interfaces. This results in cracking, ETB, and TDDB. The results show that the electrochemical activity toward water electrolysis must be considered when assessing the stability of piezo-MEMS devices in humid conditions.

II. THEORETICAL CONSIDERATIONS AND EXPERIMENTAL PROCEDURE

A. Theoretical background

The global decomposition of water (gaseous or liquid) into hydrogen and oxygen gas,

$$\text{H}_2\text{O(l, g)} \rightarrow \text{H}_2(\text{g}) + \frac{1}{2}\text{O}_2(\text{g}), \tag{1}$$
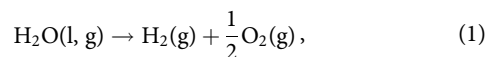
occurs via the anodic oxidation of water,

$$\text{H}_2\text{O(l, g)} \rightarrow 2\text{H}^+ + 2\text{e}^- + \frac{1}{2}\text{O}_2(\text{g}), \tag{2}$$
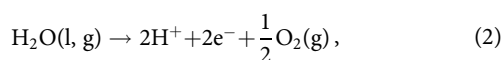
and the cathodic reduction of protons,

$$2\text{H}^+ + 2\text{e}^- \rightarrow \text{H}_2(\text{g}). \tag{3}$$

Reaction (2) is known as the oxygen evolution reaction (OER) and generally considered the rate-limiting half-reaction.[29] Reaction (3) is known as the hydrogen evolution reaction (HER).

The relationship between the electrode potential and the activity of the involved species is described using the Nernst equation,[47,48]

$$E(p, T) = E(T)^0 + \frac{RT}{n\text{F}}\ln\left(\frac{a_{\text{H}_2}\, a_{\text{O}_2}^{\frac{1}{2}}}{a_{\text{H}_2\text{O}}}\right). \tag{4}$$

Here, $E(p, T)$ is the applied voltage across the cell, $E(T)^0$ is the temperature-dependent cell potential, R is the universal gas constant, $n = 2$ is the number of electrons involved in the overall reaction of Eq. (2), F is the Faraday constant, T is the temperature, and a_n is the chemical activity of the involved species. Reaction (1) through (3) can be evaluated using Eq. (4). In humid conditions, the activity of water, $a_{\text{H}_2\text{O}}$, is given by the partial pressure of water, $p_{\text{H}_2\text{O}}$, and is unity when liquid water is present at the electrodes.[49] The solubility of O$_2$(g) and H$_2$(g) in water is low, and the activities are approximately equal to their partial pressures. According to Eq. (4), an electrochemical system will also act as an electrochemical compressor.

The thermodynamic potential for reaction (1) is 1.23 V. For large overpotentials, i.e., $\eta \gg 1.23$, the rate of an electrochemical reaction, the electrochemical activity, can be related to the overpotential using the Tafel-equations,[29,50]

$$\log_{10}|j| = a + b\eta, \quad a = \log_{10}|j_0|, \quad b = \frac{\gamma n\text{F}}{2.3RT}, \tag{5}$$

where $\eta = E - E_\text{N}$ is the overpotential required to initiate the electrolysis reaction and γ is a symmetry factor. In general, a smaller Tafel-slope, b, and larger equilibrium exchange-current density, j_0, indicate a larger electrochemical activity.

B. Experimental procedure

Undoped PbZr$_{0.52}$Ti$_{0.48}$O$_3$ (hereafter PZT) thin-films with a 90%/10% (001)/(110) grain orientation ratio were chosen as a model system for the present study. $1.72 \pm 0.07\,\mu\text{m}$ PZT thin-films, measured using a J. A. Woolam a-SE spectroscopic ellipsometer, were deposited on 6 in. platinized silicon wafers using CSD. The PZT films had a surface roughness of 11 ± 1 nm as measured by atomic force microscopy. Both top and bottom electrodes were deposited by sputtering and had a thickness of 100 nm. All top electrodes were structured into circular pads with $\varnothing = 400\,\mu\text{m}$ using lift-off, before dicing into $8 \times 8\,\text{mm}^2$ square dies. Two electrode systems commonly used for piezo-MEMS[51] were chosen based on their reported differences in electrochemical activity; Pt, a well-known and commonly utilized electrocatalyst,[24,29] and Au which is much less electrochemically active.[24] For the Pt-electrodes, a 10 nm room-temperature sputtered Ti adhesion layer and a 15 min annealing at 550 °C in O$_2$-containing atmosphere were used to improve the electrode adhesion to PZT. For the Au electrodes, a 10 nm Ti with 10 wt. % W adhesion layer was used. The final thin-film stack consisted of electrode/adhesion/PZT/LaNiO$_3$/Pt/TiO$_2$/SiO$_2$. All processing was carried out in ISO 5 cleanroom facilities.

All pads were DC-biased with a positive voltage between 2 and 40 V$_{\text{DC}}$ (10–233 kV/cm). The top electrode was intentionally chosen as the anode and directly exposed to the ambient to enable

the OER at the top electrode and HER at the bottom blanket Pt electrode. This configuration was chosen since humidity-induced degradation has been reported to occur primarily with the anode side exposed to humidity.[46] The pads were contacted using wire-bonding (wedge bonding) with a $30 \, \mu m$ gold wire for the humidity-accelerated tests. For *in situ* monitoring, using a Pixelink PL-B623 optical microscope, the pads were probed using tungsten needles.

The long-term measurements and humidity-accelerated lifetime tests, together with dielectric/ferroelectric characterization, were performed using an AixHALT system (AixACCT Systems). Capacitance–voltage measurements were done using a small-signal amplitude of 200 mV at 1 kHz. Ferroelectric hysteresis loops were measured using a large-signal amplitude of 50 V at 100 Hz. The Schottky barrier heights, Φ_B, were calculated by fitting I–V curves taken at 50 °C, 75 °C, 100 °C, 125 °C, and 150 °C to the Schottky and Poole-Frenkel equations,[11] using the refractive index of PZT, ~2.1–2.5, to determine the dominating conduction mechanism in dry ambient.[52,53] The refractive index, $n^2 = \varepsilon_\infty$, was used to select the most probable conduction mechanisms (further details in the supplementary material).[7,53] The films' transverse charge coefficient were $e_{31,f} = -14 \pm 1 \, C/m^2$, measured using the wafer flexure method with attached strain gauges.[54] Structural characterization was done using optical microscopy, scanning electron microscopy (Nova NanoSEM 650), and x-ray diffraction (Bruker AXS D8 Discover). Grain and crater sizes were determined by post-processing of the SEM images using ImageJ image analysis software.

A total of 12 pads on the same die were measured per experiment and fitted using the cumulative probability distribution function,

$$F(t; \lambda, \beta) = 1 - e^{-\left(\frac{t}{\lambda}\right)^\beta}, \quad (6)$$

where $F(t; \lambda, \beta)$ is the failure probability, t is the measured time to failure, λ is the scale, i.e., the median time to failure (MTTF), and β is the shape, describing the confidence of the measurement.[55,56] Failure by electrical breakdown was defined as the time for the leakage current to increase by two orders of magnitude compared to the steady-state leakage. TDDB measurements were conducted in controlled ambient below 50% relative humidity (RH, hereafter dry), above 95% RH (hereafter humid), and on samples immersed in DI-water (hereafter wet). The anodic electrochemical activity was assessed by fitting unidirectional I–V curves measured in humid and wet conditions to the Tafel equations [Eq. (4)]. The unidirectional I–V measurements were carried out using parameters typical for ferroelectric characterization, i.e., without a reference hydrogen electrode. A 200 mV voltage step and a 2 s dwell time per step from 0 to 10 V were used.

All measurements were conducted at room temperature (25 °C) in a compact environmental chamber fitted to the respective AixACCT characterization platforms. The ambient humidity was controlled by bubbling N_2 through DI-water and flowing the $H_2O{:}N_2$ mixture through the environmental chamber during the experiment and kept constant using a feedback loop controlled by a HYT271 humidity sensor placed next to the samples. Selected

tests were re-done using a TF3000 (AixACCT systems) for *in situ* monitoring during degradation in humid and wet conditions. More details on the environmental chamber design and experimental setup can be found in the literature.[5] The reader is directed to the supplementary material for further details on the experimental and measurement procedure.

III. RESULTS AND DISCUSSION

A. Lifetime and reliability in dry and humid conditions

The failure probability distributions for the tested electrodes in dry and humid ambient are shown in Fig. 1 and the corresponding values are summarized in Table I. The significant impact of humidity on reliability is well illustrated by comparing the median time-to-failure (MTTF) at 40 V_{DC} (~233 kV/cm) in dry and humid conditions. In dry conditions, the MTTF were 389, 528, and 417 h with a Weibull shape of 5.1, 2.0, and 5.2 for Pt/Ti/PZT, Pt/PZT, and Au/TiW/PZT, respectively. In humid conditions, the MTTF was reduced to 3 s, 4 s, and 1 h with a Weibull shape of 6.1, 3.6, and 1.1 for Pt/Ti/PZT, Pt/PZT, and Au/TiW/PZT, respectively. This is a MTTF six orders of magnitude shorter for Pt/PZT and Pt/Ti/PZT and three orders of magnitude shorter for Au/TiW/PZT in humid compared to dry operating conditions. Accordingly, the breakdown strength was reduced from 238, 503, and 472 kV/cm to 17, 27, and 111 kV/cm for Pt/Ti/PZT, Pt/PZT, and Au/TiW/PZT respectively, as shown in Table II and the supplementary material.

A typical TDDB plot at 40 V_{DC} (~233 kV/cm) is shown for dry (a) and humid (b) conditions in Fig. 2. The scanning electron microscopy (SEM) images in the inset show typical post-failure ETB events for the two conditions. In dry conditions, the leakage generally displayed a breakdown behavior consistent with a DC electrical field driven model with leakage evolving over steady-state, electrical degradation, and TDDB regimes.[14,37] Breakdown is manifested as a rapid drop in resistance across the sample and failure. In humid conditions, similar behavior was observed for the tested samples though within a drastically reduced timeframe. As shown in Fig. 1, TDDB and sample-failure in humid conditions were measured below 8 V_{DC} (~47 kV/cm). Additionally, Pt/PZT which had the highest breakdown strength and longest MTTF in dry conditions displayed similar TDDB-behavior and MTTF as Pt/Ti/PZT in humid conditions. In comparison, Au/TiW/PZT exhibited three orders of magnitude of time longer MTTF than both Pt/PZT and Pt/Ti/PZT in humid conditions. Sub-coercive driving-voltages (here in the order of 45 kV/cm) generally result in piezoelectric stresses well below typical crack initiation stresses for polycrystalline PZT, which can range from 450 to 600 MPa.[57–59] For the present films the average residual stress was 100 MPa, which together with the piezoelectric stress ($\sigma_P = -e_{31,f}E_z$) under an applied field of 4 and 8 V, amounts to a total stress of approximately 127 MPa and 155 MPa, respectively. Failure due to piezoelectrically induced mechanical cracking is thus not to be expected, suggesting a different mechanism controlling humidity-induced degradation.

Post-breakdown SEM, as exemplified in the inset of Fig. 2, shows typical ETB craters of samples failed under dry and humid conditions, respectively. Elemental mapping (see the supplementary material) shows traces of all elements in the stack, including Si, both inside the crater and scattered on the surrounding PZT and

FIG. 1. Failure probability distributions in dry and humid conditions for (a) Au/TiW/PZT, (b) Pt/PZT, and (c) Pt/Ti/PZT. The corresponding shape and scale-parameters are given in Table I.

between dry and humid conditions. While the overall crater size on samples failed in dry conditions was in the order $3\,\mu m^2$ regardless of the type of electrode, the overall crater size in humid conditions was in the order of $300\,\mu m^2$ and dependent on the electrode system. This suggests that different mechanisms provoke ETB in humid and dry ambient, which will be further discussed below.

In dry conditions, degradation of PZT thin-films is often connected to the properties of the electrode interface and typically dominated by either Schottky and/or Poole–Frenkel emission.[7,10,60,61] It is plausible that the properties of the interface barriers can be altered as a result of interactions between the layer stack and water. In the present study, this can, e.g., be due to the oxidation of the Ti- and W-based adhesion layer to TiO_{2-x} or WO_{3-x},[62–64] driving the observed degradation.[34,39,65,66] Based on I–V measurements in dry ambient, it is shown, see the supplementary material, that for a positive DC bias of the top electrode, the conduction is Schottky-limited with barrier heights of $\Phi_{Pt} = 0.77$, $\Phi_{Au/TiW} = 0.65$, and $\Phi_{Pt/Ti} = 0.59\,eV$ for Pt/PZT, Au/TiW/PZT, and Pt/Ti/PZT, respectively (see Table II). This is consistent with n-type electrode systems at both top and bottom interfaces, and comparable with theoretical predictions for barrier heights.[63,67,68] Since such I–V measurements represent the total leakage arising from charge-injection across both the top and bottom electrodes, the overall leakage will be sensitive to the characteristics of both interfaces. In dry conditions, the average breakdown strength and MTTF, being largest for Pt/PZT and smallest for Pt/Ti/PZT top electrodes, suggests that degradation could be related to possible degradation of the electrode interfaces.[12,14,15,61,69–71] In humid conditions, on the other hand, the breakdown strength and MTTF of the Pt/PZT top electrode, which should not have an interfacial oxidized layer, are comparable to that of Pt/Ti/PZT, inconsistent with degradation of the barrier height at the top electrode interface.

B. Time-evolution of degradation in humid and wet conditions

Based on the reliability data obtained in dry and humid conditions combined with the hypothesis that water-electrolysis plays a key role in the degradation process, additional TDDB measurements were conducted in wet conditions and compared with TDDB measurements in humid conditions. Selected samples were monitored by optical microscopy *in situ* during degradation to investigate the degradation process in more detail. Since, in humid conditions, operation at $40\,V_{DC}$ induced instantaneous sample failure, degradation with a DC bias of $2-20\,V_{DC}$ ($\sim 12-116\,kV/cm$) was studied in more detail in both humid and wet conditions. For illustration purposes, degradation as a function of time is exemplified for a set of samples degraded at $10\,V_{DC}$ in humid and wet conditions in Fig. 3, noting that similar TDDB characteristics were encountered for the other voltages over different time scales. In Fig. 3, the leakage vs time and *in situ* optical microscopy are shown for humid conditions in (a) and (b) and for wet conditions in (c) and (d).

In humid conditions, degradation generally evolved over three stages, indicated explicitly for Pt/Ti/PZT in Fig. 3(a). Stage 1 was associated with a steady-state leakage and few leakage transients. It is assumed that minor transients originate from temporary surface

electrode surface. This is consistent with similar breakdown-events reported in the literature,[15,19,21] in which the dissipation of high power densities locally sublimate the stack material. The considerable difference in post-failure crater size is a key distinction

TABLE I. Measured probability failure parameters for Fig. 1; α is the Weibull scale and κ the Weibull shape. The 95% confidence interval is given in the brackets.

Electrode	40 V, dry	40 V, humid	20 V, humid	10 V, humid	8 V, humid
Pt/PZT	$\kappa = 5.1/\alpha = 1.9 \times 10^6$ $[1.4 \times 10^6 - 2.1 \times 10^6]$	$\kappa = 6.1/\alpha = 4.0 \times 10^0$ $[3.7 \times 10^0 - 4.5 \times 10^0]$	$\kappa = 1.0/\alpha = 4.8 \times 10^3$ $[2.7 \times 10^3 - 8.8 \times 10^3]$	$\kappa = 0.9/\alpha = 1.1 \times 10^4$ $[5.1 \times 10^3 - 2.4 \times 10^4]$	$\kappa = 1.2/\alpha = 2.2 \times 10^4$ $[1.1 \times 10^4 - 4.5 \times 10^4]$
Pt/Ti/PZT	$\kappa = 2.0/\alpha = 1.4 \times 10^6$ $[1.1 \times 10^6 - 1.9 \times 10^6]$	$\kappa = 3.6/\alpha = 3.3 \times 10^0$ $[2.8 \times 10^0 - 3.9 \times 10^0]$	$\kappa = 1.1/\alpha = 1.9 \times 10^3$ $[1.2 \times 10^3 - 3.2 \times 10^3]$	$\kappa = 1.2/\alpha = 2.9 \times 10^3$ $[1.6 \times 10^3 - 5.2 \times 10^3]$	$\kappa = 1.2/\alpha = 7.5 \times 10^3$ $[4.1 \times 10^3 - 1.2 \times 10^4]$
Au/TiW/PZT	$\kappa = 5.1/\alpha = 1.5 \times 10^6$ $[1.4 \times 10^6 - 1.7 \times 10^6]$	$\kappa = 1.1/\alpha = 3.2 \times 10^3$ $[2.0 \times 10^3 - 5.2 \times 10^3]$	$\kappa = 1.4/\alpha = 9.6 \times 10^3$ $[6.1 \times 10^3 - 1.5 \times 10^4]$	$\kappa = 1.9/\alpha = 1.2 \times 10^4$ $[9.0 \times 10^3 - 1.7 \times 10^4]$	$\kappa = 2.6/\alpha = 2.8 \times 10^4$ $[1.9 \times 10^4 - 3.9 \times 10^4]$

currents combined with initial microcracking and partial delamination as shown in the corresponding *in situ* image of Fig. 3(b) for all electrode systems. For Pt/Ti/PZT, delamination-points were observed as gas pockets under the top electrode, while for Pt/PZT and Au/TiW/PZT, hollow channels formed underneath the top electrodes, inducing larger and more prominent cracks. Degradation stage 2 was generally characterized by multiple leakage transients and cracking before the onset of ETB events along newly formed cracks, as shown in the *in situ* recordings of Fig. 3(b). The measured transient currents had an amplitude in the μA–mA range, consistent with previous literature reports.[21,22,26,45] Degradation stage 3 was characterized by a rapid increase in the number of cracks propagating and growing in size, more leakage transients added to an increasing background leakage, and an increased frequency of ETB events. Altogether such events eventually lead to sample failure by TDDB.

In wet conditions, Figs. 3(c)–3(d), the leakage currents were considerable larger, reflecting an increased activity on the samples immersed in water. Furthermore, consistent with their higher reported electrochemical activity, the initial leakage current was about one order of magnitude larger for Pt/Ti/PZT and Pt/PZT than for Au/TiW/PZT. As shown in Fig. 3(c), differences were also found in the three degradation stages, compared to humid conditions. During degradation stage 1 in wet conditions, the leakage increased together with an increase in the amount of gas evolving on the anode and cathode side of the stack. From the *in situ* measurements, it was found that gas initially emerged from the top electrode followed by gas emerging from the surrounding surfaces of the PZT film, consistent with the anodic OER and cathodic HER of an electrochemical cell. It is noted that both the current density and the amount of bubbling were always considerably smaller for Au/TiW/PZT than for Pt/PZT and Pt/Ti/PZT during degradation stage 1. Although the concentration of cracks was highest underneath and around the used electrode, it is also notable that bubbles emerged across the entire die during degradation, including from underneath the unused electrodes. This suggests that a consequence of using a blanket bottom electrode, preferred nucleation-points for evolving H_2(g) from half-reaction (3) may form over the entire die, even at large distances from the electrode used. This is consistent with the fact that small changes in the microstructure may significantly influence the transport mechanism and the mobility of protons.[32,33,72,73] In this scenario, microstructural features, such as chemical defects, grain boundaries, grooves, microcracks, etc. will influence the transport of protons, and the nucleation points for evolution of H_2(g). Altogether, such mechanisms will be detrimental for the rate of humidity-accelerated degradation.

Degradation stage 2 in wet conditions was associated with increased leakage, cracking, and an increased amount of gas emerging from the PZT and electrode surfaces. The early onset of degradation stage 2 on the Pt-based electrodes compared to the Au-based electrodes is clearly shown in Figs. 3(c)–3(d); this correlates well with their comparatively higher catalytic properties. Here, at 10 V_{DC}, the time for onset of stage 2 degradation were in the order of 20, 900, and 4600 s for Pt/Ti/PZT, Pt/PZT, and Au/TiW/PZT, respectively, though with relatively large standard deviations (Table II). At degradation stage 3, the formation of new cracks stopped, and the system reached a steady-state leakage current and gas evolution across the die. As shown in Fig. 3(d), the Pt-based electrodes displayed more vigorous bubbling and a significantly larger steady-state leakage in comparison to the Au-based electrodes, in line with the above discussion. It is noted that neither ETB nor craters were found post-failure in wet conditions. This observation is ascribed to two effects. First, the surrounding water will cool the die and reduce Joule heating in the case of an ETB. Second, upon cracking, the new dielectric medium separating the top and bottom electrodes in humid conditions will include humidified air which has a breakdown strength of 30 kV/cm. In wet conditions, the new dielectric medium will include distilled water with a breakdown-strength of 650–700 kV/cm. Comparing these values to the dry-condition breakdown-strengths of 240–500 kV/cm, opening a crack will more easily result in dielectric

TABLE II. Electrical and structural properties in dry and humid conditions.

Electrode	E_C (kV/cm) dry	Φ_B (eV) dry	BDS (kV/cm) dry	BDS (kV/cm) humid	$A_{ETB}(\mu m^2)$ dry	$A_{ETB}(\mu m^2)$ humid
Pt/PZT	45.3 ± 0.4	0.77 ± 0.06	503.4 ± 52.7	27.5 ± 2.9	3.7 ± 1.0	317.9 ± 125.4
Pt/Ti/PZT	45.6 ± 0.1	0.59 ± 0.11	237.5 ± 51.7	17.3 ± 9.8	3.1 ± 0.9	30.2 ± 18.1
Au/TiW/PZT	49.5 ± 4.2	0.65 ± 0.09	471.5 ± 30.6	111.7 ± 10.3	2.5 ± 1.5	466.6 ± 223.8
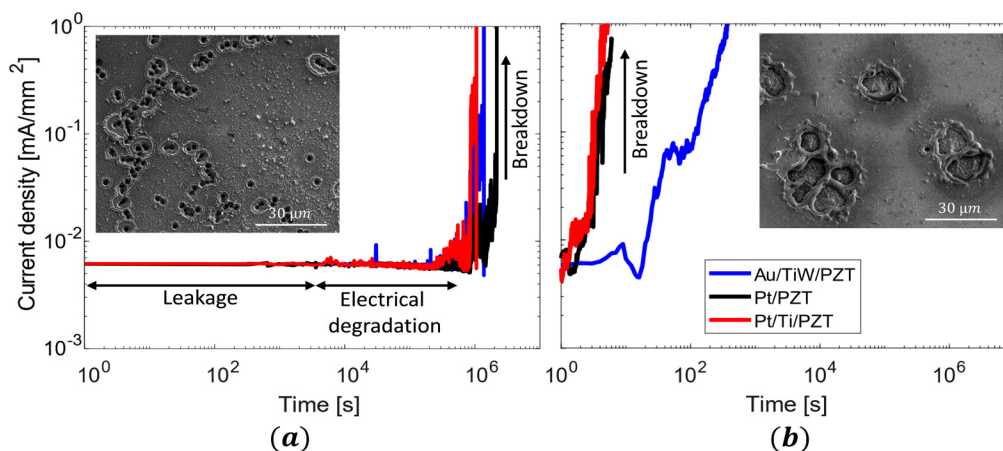
FIG. 2. Comparison of leakage vs time at 40 V_{DC} for Au/TiW/PZT (blue), Pt/PZT (black), and Pt/Ti/PZT (red) in dry (a) and humid (b) conditions. The inset SEM image shows typical sizes of the post-breakdown ETB-craters, generally found to be significantly larger in humid compared to dry conditions, independent of electrode-system.
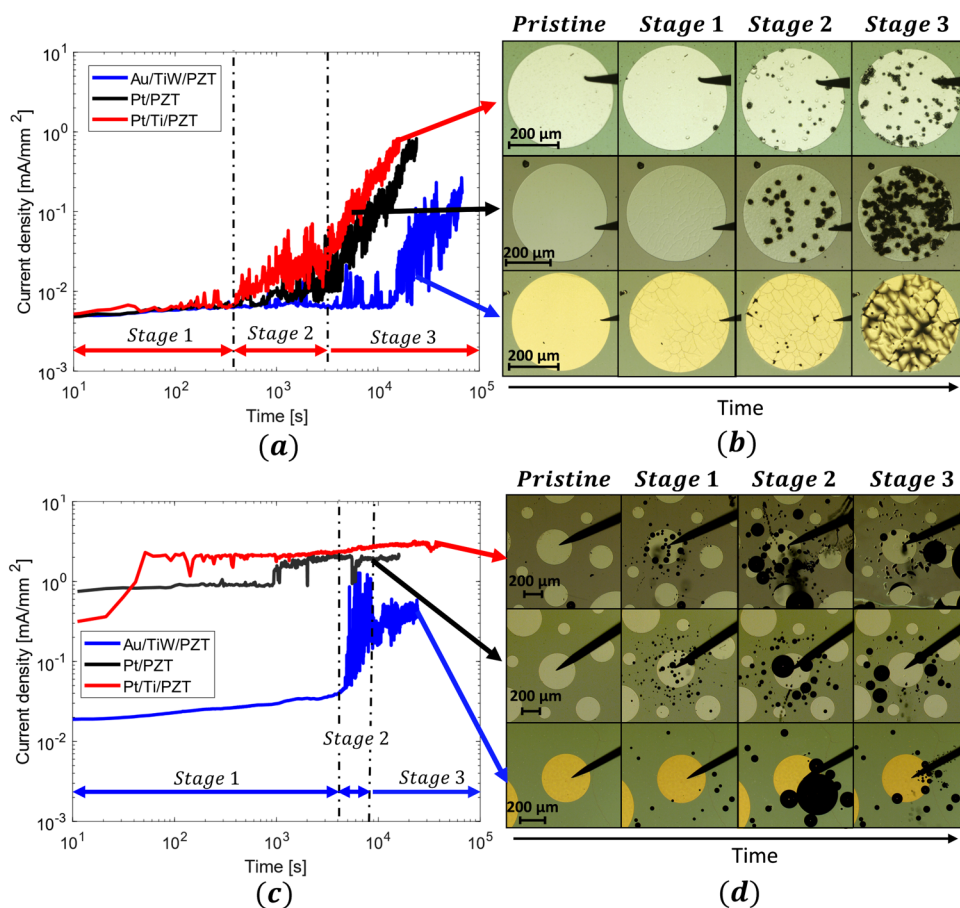
FIG. 3. Electrochemical degradation exemplified by typical time-evolution of leakage current and corresponding *in situ* optical images for Au/TiW/PZT (blue), Pt/PZT (black), and Pt/Ti/PZT (red) for potentials exceeding E_2 (here 10 V_{DC}) in humid (a) and (b) and wet (c) and (d) conditions. The three stages of degradation are indicated for Au/TiW/PZT. The circular black features in (d) are bubbles forming on the surface because of water-electrolysis.
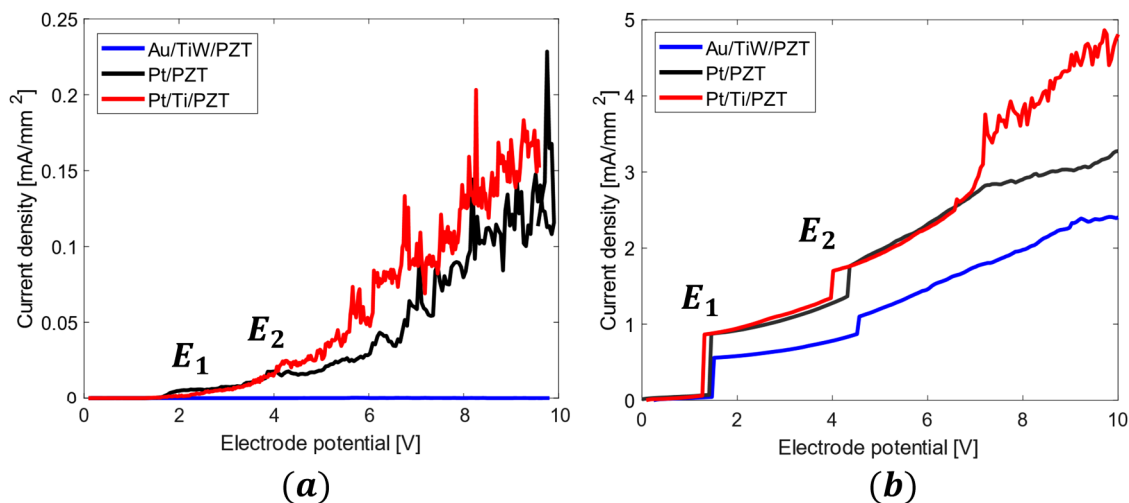
FIG. 4. Examples of unidirectional I-V measurements for Au/TiW/PZT (blue), Pt/PZT (black), and Pt/Ti/PZT (red) in humid (a) and wet (b) conditions. The apparent overpotentials are indicated by E_1 and E_2, respectively.

breakdown and ETB. For the present study, the applied fields exceed the breakdown strength of air above a DC bias of approximately 5 V, which correlates well with ETB appearing below 8 V_{DC} for the present stack in humid conditions.

C. Electrochemically driven degradation

Since a complete electrochemical cell is needed for reaction (1) to commence, the evolution of bubbles on the electrodes in wet conditions is direct evidence for the transport of protons from the anode to the cathode side of the stack.[32,74–76] Here, the electrolyte is the combination of the PZT film and surface water. The electrochemical activity of the system is determined by the electrode kinetics in the electrochemical cell, in which the OER is generally accepted as the rate-limiting half-reaction.[32,33,72,77,78] The electrochemical activity of the present system was therefore investigated using I–V measurements with respect to an anodic top electrode (OER). Example measurements for humid and wet conditions are shown in Figs. 4(a) and 4(b). The results are summarized in Table III. The presented data highlights important effects of the electrode characteristics, yet it should be noted that accurate electrochemical characterization requires well-defined activities of reactants/products, particularly for H_2 at the bottom electrode, and a reference electrode.[29,50,79] Evaluation of the exact overpotentials,

other contributing electrochemical reactions, such as the reduction of surface oxide species at the metal electrodes, the electrochemical contributions to the measured leakage current (faradaic efficiency), the contributions from surface currents, etc. are left for future studies.

The I–V measurements in Fig. 4 distinguishes important features related to the electrochemical activity of the layer stack. First, the measured current densities were always significantly larger for wet conditions compared to humid conditions. This is consistent with the increased activity of H_2O at the anode side, resulting in an increased transport of protons from the anode to the cathode through the electrolyte. Second, the current density was always larger for Pt/Ti/PZT and Pt/PZT compared to Au/TiW/PZT when exceeding the apparent onset potential for the electrolysis reaction, denoted E_1 in Figs. 4(a) and 4(b). This was true for both humid and wet conditions. Third, exceeding E_1 in wet conditions was always associated with the evolution of oxygen gas at the anode side, see Fig. 3(d) and the supplementary videos in the supplementary material. Altogether, this provides both direct evidence for the complete electrolysis reaction [Eq. (1)] and a demonstration that the electrochemical activity was larger for Pt/Ti/PZT and Pt/PZT than for Au/TiW/PZT. Here, using voltage steps of 200 mV, E_1 appears as steps in the I-V curves in both humid and wet conditions. It is noted that when the voltage resolution is increased, these apparent steps will appear as a continuous,

TABLE III. Measured electrochemical properties of the electrode systems.

Electrode	E_1 (V) wet	E_2 (V) wet	b (mV/dec) wet	$\Delta j(E_1)$ (mA/mm²) wet	$\Delta j(E_2)$ (mA/mm²) wet	γ wet	E_1 (V) humid
Pt/PZT	1.5 ± 0.3	4.5 ± 0.2	285 ± 16	0.9 ± 0.3	0.5 ± 0.1	0.6 ± 0.3	1.8 ± 0.2
Pt/Ti/PZT	1.4 ± 0.2	4.5 ± 1.7	259 ± 5	1.1 ± 0.4	0.6 ± 0.2	0.5 ± 0.3	1.8 ± 0.4
Au/TiW/PZT	1.6 ± 0.1	4.3 ± 0.2	376 ± 33	0.4 ± 0.2	0.3 ± 0.1	1.1 ± 0.4	N/A

rapid increase in the current density starting from E_1. In humid conditions, E_1 was 1.8 V for both Pt/PZT and Pt/Ti/PZT, whereas no clear onset potentials or exponential increase in current densities could be measured for Au/TiW/PZT. In wet conditions, E_1 was 1.5 V for all electrode systems within the measurement error (Table III). The lower apparent onset potential in wet conditions is reasonable considering the increased activity of water.

For potentials exceeding E_1, the current density increased exponentially with voltage for all electrode systems in both humid and wet conditions, consistent with the Butler-Volmer formalism. By fitting the data from wet conditions for $V \gg E_1$ to Eq. (5), slopes of $b_{Pt} = 286$ mV/dec, $b_{Pt/Ti} = 259$ mV/dec, and $b_{Au/TiW} = 376$ mV/dec with corresponding equilibrium current densities of $\Delta j_{Pt}(E_1) = 0.9$ mA/mm^2, $\Delta j_{Pt/Ti}(E_1) = 1.1$ mA/mm^2, and $\Delta j_{Au}(E_1) = 0.4$ mA/mm^2, were found for Pt/PZT, Pt/Ti/PZT, and Au/TiW/PZT, respectively (see Table III). In humid conditions, exceeding E_1 was associated with significant cracking, delamination and ETB. Spontaneous failure was frequently observed for the Pt/PZT and Pt/Ti/PZT samples, presumably due to dielectric breakdown through air upon cracking as discussed above. In contrast, less cracking, no spontaneous failures and small sample-to-sample variations were measured for Au/TiW/PZT, consistent with the electrochemical data. However, as a consequence, no adequate fits to Eq. (5) could be made for samples in humid conditions. It is noted that the overall characteristics were comparable with wet conditions as shown in Fig. 4(a).

D. Effects of electrochemical compression

It is directly demonstrated in this study that $O_2(g)$ and $H_2(g)$ evolve when the systems' onset potential for water electrolysis is exceeded. If the gaseous species are trapped at the interfaces, a pressure will be exerted on the PZT-film and electrodes as the reaction proceeds. By assuming that the majority of the $O_2(g)$ bubbles evolving at the anode can escape freely, the oxygen activity, a_{O_2}, can be set to unity. Setting $a_{H_2O} = p_{H_2O}$ allows for an estimation of the pressure build-up due to $H_2(g)$ evolving at the bottom blanket electrode from Eq. (4).[32,49,80,81] In Figs. 4(a) and 4(b), a second apparent onset potential, E_2, is indicated. From *in situ* microscopy, E_2 was found to coincide with the cracking of the PZT immediately releasing pockets of trapped gas from underneath the electrodes and the surrounding PZT surface in wet conditions. For an ideal system under standard conditions, disregarding increased resistance due to the increase in cathode pressure, an increase of the top

electrode potential of 34 mV is needed per decade increase of cathode pressure. The measured apparent overpotential E_2 appears around 3 V above E_1 for all electrode systems, corresponding to a maximum pressure of approximately 880 MPa. This is in reasonable agreement with crack initiation stresses of PZT prepared by CSD, 450–600 MPa,[59] subject to the microstructural characteristics of the specific sample. The measured increase in leakage (resistance drop) associated with cracking; $\Delta j_{Pt/Ti}(E_2) = 0.6$ mA/mm^2, $\Delta j_{Pt}(E_2) = 0.5$ mA/mm^2, and $\Delta j_{Au}(E_2) = 0.3$ mA/mm^2, can be associated with a reduced Nernst potential due to cathodic pressure relief upon cracking.[73] The measured resistance drop due to cracking will depend on the nature and severity of cracking.

E. Pressure build-up, cracking, and breakdown in humid conditions

To investigate the coupling between humidity degradation and cracking, the humidity-degradation process was interrupted partway for selected samples. The top electrodes were subsequently removed by wet etching and the samples analyzed by SEM to investigate whether cracks were only present in the top electrode, or if both the PZT film and electrode were affected. Cracks were found in the PZT on all humidity-degraded samples, however not necessarily coinciding with ETBs as has been observed in the literature.[15] The largest cracks were found on Pt/PZT and Au/TiW/PZT, together with considerably larger post-failure craters compared to Pt/Ti/PZT. This is exemplified in the SEM-images of post-degraded samples in Figs. 5(a)–5(c) and tabulated in Table II. Overall, the average ETB crater sizes assessed using the ImageJ software,[82] were 470, 30, and 320 μm^2 for Pt/PZT, Pt/Ti/PZT, and Au/TiW/PZT, respectively. Also, characteristic for Pt/Ti/PZT was a significantly smaller crater size compared to the amount of the top electrode removed, compared to Pt/PZT and Au/TiW/PZT, in which the amount of removed top electrode area was generally comparable to the ETB crater size. From tape pull-tests, it was found that the electrode adhesion strength was generally considerably lower with Ti as an adhesion layer compared to TiW or annealed Pt electrodes for the present samples. This could originate from an oxidized layer of TiO_{2-x} at the Ti/PZT-interface, since no pre-deposition bakeout procedure was used before depositing the adhesion layer. As a result of the lower adhesion strength, the Pt/Ti/PZT electrode delaminates more easily, allowing for a build-up of gas pockets underneath the top electrode, as shown for Pt/Ti/PZT in Figs. 3 and 6(b).
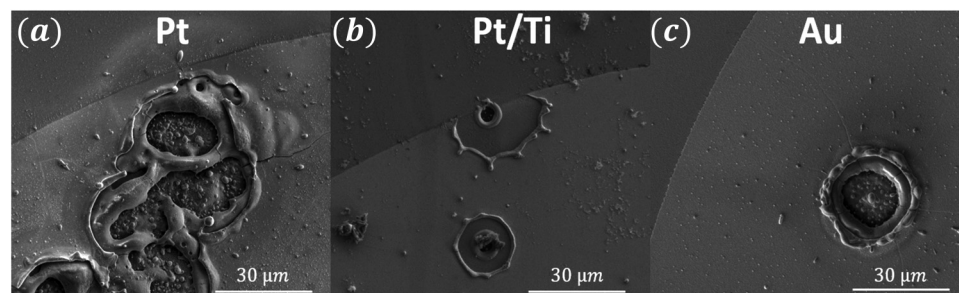
FIG. 5. Comparison of post-breakdown ETB-crater-sizes for Pt/PZT (a), Pt/Ti/PZT (b), and Au/TiW/PZT (c) in humid conditions.
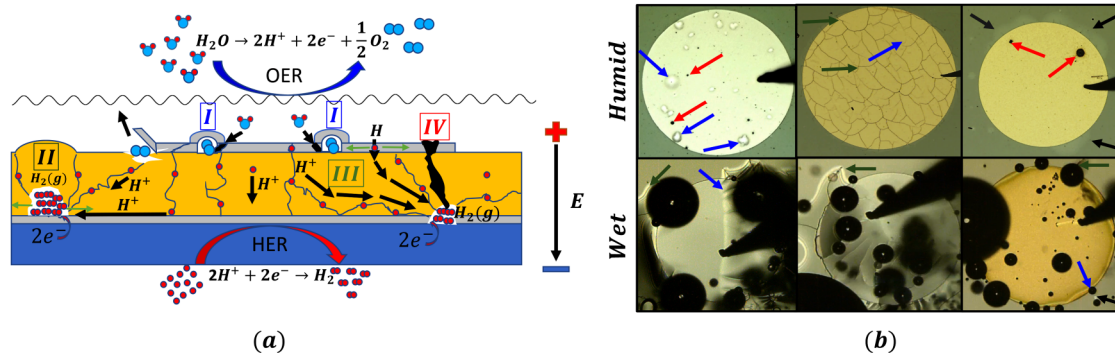
FIG. 6. Schematic representation of electrochemically driven degradation in humid ambient (a) and examples of the proposed mechanisms observed *in situ* indicated by the color of the arrow for humid and wet conditions (b). Several events occur as indicated by the colored numbers: (I) $O_2(g)$ evolves between the anode and the cathode (blue arrows); (II) $H_2(g)$ evolves between the electrolyte and cathode and between cathode and Si (black arrows); (III) cathodic $H_2(g)$ increases the internal pressure until the critical stress of the film is exceeded and cracks are initiated (green arrows); (IV) resulting electrothermal breakdown-events in humid conditions (black arrows) and cracking in wet conditions.

Altogether this correlates well with dielectric breakdown through air in the cracks, suggesting that different electrode and film characteristics, and, in particular, the electrode adhesion strength, influence degradation in humid conditions. While dry conditions, degradation is driven by migrating species, electrochemical compression drives degradation in humid conditions. For pressure to build up during electrolysis, water or gaseous species must be trapped at the interfaces, which raises questions regarding entry-points for water and nucleation-points for gas to evolve. Though not explicitly shown here, minor defects such as pinholes, cracks, grooves, and voids, were present at all electrodes, post-processing. From recent studies on surface protonics,[32,33,72,73] it has been shown that grain boundaries, microcracks, and grooves act as high-mobility channels for proton transport. Minor defects in the electrode which do not affect reliability in dry conditions, do influence reliability of piezo-MEMS in humid conditions.

This claim is further supported by the appearance of gas pockets on the electrode surface of the Pt/Ti/PZT electrode systems. As a consequence of the poor adhesion strength, the exerted pressure between the top electrode is partially relieved around electrode delamination points. As a lower pressure is needed to form a gas pocket underneath the electrode, the underlying PZT layer will be less affected, decreasing the size of both cracks and the ETBs compared to Pt/PZT and Au/TiW/PZT, which exhibit considerably better adhesion strength. This is shown in Figs. 3 and 6(b). As indicated by the black arrows in Fig. 6(b), similar trends were observed for Au/TiW/PZT. A distinct difference is the appearance of gas-pockets at the PZT/Pt bottom electrode interface combined with gas pockets at the top electrode interface. This further supports proton transport through the PZT film, possibly related to the hydration of oxygen vacancies.[32,38] It is suggested that more delamination occurs away from the Au/TiW/PZT electrode due to the longer degradation time in humid conditions compared to Pt/Ti/PZT and Pt/PZT. That is, since the water decomposition rate is lower, protons have more time to drift, nucleate, and spread along the blanket bottom electrode prior to cracking and ETB.

An implication of the mechanisms discussed here for piezo-MEMS operating under unipolar excitation exceeding 5 V is that once initiated, humidity-related degradation can propagate and severely degrade even well-protected devices.

F. Degradation model

The presented data show that degradation in humid conditions is driven by water electrolysis and electrochemical compression. A proposed degradation model explaining the processes involved in the degradation are schematically illustrated in Fig. 6(a). Examples from *in situ* optical measurements are shown in (b), with the colored arrows pointing to the various types of events in the schematic; blue indicates top electrode delamination, red ETB, green cracking, and black PZT/bottom electrode delamination. As discussed above, the layer stack acts as an electrolytic cell in humid or wet conditions. Water electrolysis initiates above an onset potential, enabling the anodic generation of $O_2(g)$ and H^+ via the OER [Eq. (2)]. Though most of the evolved gas will escape directly from the anode surface, $O_2(g)$ can evolve from trapped water underneath the anode, causing local pressure build-up. Eventually, the exerted pressure causes the electrode to delaminate and the film to crack, denoted (I) in Fig. 6(a) and exemplified for Pt/Ti/PZT and Au/TiW/PZT by the blue arrows in Fig. 6(b). Protons formed at the anode will drift toward the cathode. Anode–cathode pathways may form both through the film and along the surface since a blanket Pt bottom electrode is used. Microstructural features such as voids, grooves, and cracks in the PZT material, together with stray fields and the presence of adsorbed surface water can allow protons to drift and form $H_2(g)$ across the entire die. This is illustrated by [II] in Fig. 6(a) and exemplified by the black arrows in (b). Cathodic generation of $H_2(g)$ occurs as protons are reduced via the HER [Eq. (3)] at a rate depending on the kinetics of the electrochemical system. As cathodic $H_2(g)$ evolves, the internal pressure on PZT increases, eventually exceeding the critical stress of PZT to initiate cracking and accelerate degradation, as illustrated by [III] (green arrows).[58] Initially, the proton concentration and hence the rate of $H_2(g)$ evolution at the cathode is small since

protons must move through the PZT film via microstructural defects, grain boundaries or bulk. Upon cracking, the conductivity of protons increases as a consequence of a transition from solid-state proton diffusion to proton conduction in surface water and confined channels.[13,72,74,78] When cracks become large enough to allow air or water, the new dielectric medium separating the top and bottom electrode will dictate the appearance of ETB events. As a result of air having a lower dielectric strength than PZT, dielectric breakdown will occur through humidified air in cracks as indicated by (IV) in (a) and exemplified by the red arrows in (b). As ETBs allows for additional pathways for protons to move to the cathode, a cascade of ETB will eventually lead to TDDB. In general, the proposed degradation model may apply to other dielectric systems under bias in humid conditions as long as an ionic conduction path can develop between the electrodes.

IV. CONCLUSIONS

Three electrode systems commonly used for PZT-based piezo-MEMS devices—Au/TiW/PZT, Pt/PZT, and Pt/Ti/PZT—were studied due to their differences in reported electrochemical activity toward water electrolysis. It was shown that the electrolysis of water and electrochemical compression drives the degradation in humid and wet conditions. Thus, the dominating degradation mechanism differs fundamentally from those encountered in dry conditions and depends on the electrochemical activity of the layer-stack toward water electrolysis.

In dry conditions at room temperature, the median time to failure at $40\,V_{DC}$ and the breakdown strength was $1.5 \times 10^6\,s$ and $471\,kV/cm$, $1.9 \times 10^6\,s$ and $503\,kV/cm$ and $1.4 \times 10^6\,s$ and $237\,kV/cm$ for Au/TiW/PZT, Pt/PZT, and Pt/Ti/PZT, respectively. This correlated well with the calculated Schottky barrier heights of $\Phi_{Au/TiW} = 0.65\,eV$, $\Phi_{Pt} = 0.77\,eV$, and $\Phi_{Pt/Ti} = 0.59\,eV$, suggesting an electrical field driven degradation in dry ambient. In humid conditions, the measured median time to failure at $40\,V_{DC}$ and breakdown strengths were reduced to $3.2 \times 10^3\,s$ and $111\,kV/cm$, $4.0\,s$ and $28\,kV/cm$ and $3.3\,s$ and $17\,kV/cm$ for Au/TiW/PZT, Pt/PZT, and Pt/Ti/PZT, respectively, consistent with an electrochemical driving force for degradation.

From unidirectional I–V measurements, it was found that the electrochemical activity toward water electrolysis was largest for the Pt-based electrode systems in both humid and wet conditions. An apparent onset potential for the electrolysis of water, $H_2O(l) \rightarrow H_2(g) + \frac{1}{2}O_2(g)$, was measured at $1.8\,V$ in humid conditions and $1.5\,V$ in wet conditions. A second onset potential of $E_2 = 4.5\,V$ coincided with cracking of the PZT film, indicating that the built-up pressure from evolved gas at the anode and cathode exceeded either the critical stress of PZT to induce cracking, or the pressure needed to cause electrode delamination. The crater sizes due to the electrothermal breakdown events were found to be significantly larger in humid compared to dry conditions and absent in wet conditions. This was ascribed to the combination of the crack size and the breakdown strength of the dielectric separating the top and bottom electrode upon cracking. A degradation model to explain the observed phenomena was proposed, taking into account water electrolysis and electrochemical compression as the main driving forces for degradation in humid conditions.

SUPPLEMENTARY MATERIALS

See the supplementary material for additional aspects related to the experimental setup, ferroelectric properties, film microstructure, Schottky-barrier measurements, degradation in dry, humid, and wet conditions, electrochemical activity, and recovery from humidity-related degradation. The supplementary videos compare the degradation dynamics of the tested electrode systems in dry, humid, and wet conditions.

DATA AVAILABILITY

The data that support the findings of this study are available from the corresponding author upon reasonable request.

REFERENCES

[1]T. Bakke, A. Vogl, O. Zero, F. Tyholdt, I. R. Johansen, and D. Wang, J. Micromech. Microeng. **20**, 064010 (2010).
[2]S. Trolier-McKinstry, S. Zhang, A. J. Bell, and X. Tan, Annu. Rev. Mater. Res. **48**, 191 (2018).
[3]R. Bogue, Sens. Rev. **33**, 300 (2013).
[4]A. Arab and Q. Feng, Int. J. Adv. Manuf. Technol. **74**, 1679 (2014).
[5]R.P. Dahl-Hansen, T. Tybell, and F. Tyholdt, in 2018 IEEE ISAF-FMA-AMF-AMEC-PFM International Conference IFAAP 2018 (IEEE, 2018), pp. 1–4.
[6]R.Q. Rudy, L.M. Sanchez, M. Tellers, and R.G. Polcawich, in 2015 Transducers —2015 18th International Conference on Solid-State Sensors, Actuators Microsystems (IEEE, 2015), pp. 1315–1317.
[7]L. M. Garten, M. Hagiwara, S. W. Ko, and S. Trolier-McKinstry, Appl. Phys. Lett. **111**, 122903 (2017).
[8]T. J. M. Bayer, J. J. Wang, J. J. Carter, A. Moballegh, J. Baker, D. L. Irving, E. C. Dickey, L. Q. Chen, and C. A. Randall, Acta Mater. **117**, 252 (2016).
[9]G. W. Dietz, W. Antpöhler, M. Klee, and R. Waser, J. Appl. Phys. **78**, 6113 (1995).
[10]A. Klein, J. Am. Ceram. Soc. **99**, 369 (2016).
[11]F. Chiu, Adv. Mater. Sci. Eng. **2014**, 578168 (2014).
[12]B. Akkopru-Akgun, W. Zhu, C. A. Randall, M. T. Lanagan, and S. Trolier-Mckinstry, APL Mater. **7**, 120901 (2019).
[13]F. Messerschmitt, M. Jansen, and J. L. M. Rupp, Adv. Electron. Mater. **4**, 1800282 (2018).
[14]Y. A. Genenko, J. Glaum, M. J. Hoffmann, and K. Albe, Mater. Sci. Eng. B Solid State Mater. Adv. Technol. **192**, 52 (2015).
[15]W. Zhu, T. Borman, K. DeCesaris, B. Truong, M. M. Lieu, S. W. Ko, P. Mardilovich, and S. Trolier-McKinstry, J. Am. Ceram. Soc. **102**, 1734 (2018).
[16]W. Zhu, B. Akkopru-Akgun, and S. Trolier-McKinstry, Appl. Phys. Lett. **111**, 212903 (2017).

[17]B. Akkopru-Akgun, W. Zhu, M. T. Lanagan, and S. Trolier-McKinstry, J. Am. Ceram. Soc. **102**(9), 5328 (2019).

[18]C. Slouka, T. Kainz, E. Navickas, G. Walch, H. Hutter, K. Reichmann, and J. Fleig, Materials **9**, 945 (2016).

[19]J. Wang, C. Salm, E. Houwman, M. Nguyen, and J. Schmitz, Proc. 2016 IEEE Int. Integr. Reliab. Work. IIRW 2016 **0**, 65 (2017).

[20]A. Bahramian, M. Eyraud, F. Vacandio, and P. Knauth, Microelectron. Eng. **206**, 25 (2019).

[21]I. P. Lipscomb, P. M. Weaver, J. Swingler, and J. W. McBride, J. Electroceramics **23**, 72 (2009).

[22]D. Zheng, M. Luo, and J. Swingler, Sensors Actuators A Phys. **241**, 197 (2016).

[23]W. P. Chen, H. L. W. Chan, F. C. H. Yiu, K. M. W. Ng, and P. C. K. Liu, Appl. Phys. Lett. **80**, 3587 (2002).

[24]Z. Chen, D. Cummins, B. N. Reinecke, E. Clark, M. K. Sunkara, and T. F. Jaramillo, Nano Lett. **11**, 4168 (2011). 3

[25]C. Zhang, H. He, and K. Ichi Tanaka, Appl. Catal. B Environ. **65**, 37 (2006).

[26]I. P. Lipscomb, P. M. Weaver, J. Swingler, and J. W. McBride, Sensors Actuators A Phys. **151**, 179 (2009).

[27]J. Chen, H. Arandiyan, X. Gao, and J. Li, Catal. Surv. Asia **19**, 140 (2015).

[28]N. M. Martin, N. Nilsson, M. Skoglundh, E. C. Adams, X. Wang, G. Smedler, A. Raj, D. Thompsett, G. Agostini, S. Carlson, K. Norén, and P.-A. Carlsson, Catal. Struct. React. **3**, 24 (2017).

[29]T. Shinagawa, A. T. Garcia-Esparza, and K. Takanabe, Sci. Rep. **5**, 1 (2015).

[30]M. H. Miles, E. A. Klaus, B. P. Gunn, J. R. Locker, W. E. Serafin, and S. Srinivasan, Electrochim. Acta **23**, 521 (1978).

[31]M. H. Miles, J. Electrochem. Soc. **123**, 1459 (2006).

[32]SØ Stub, E. Vøllestad, and T. Norby, J. Phys. Chem. C **121**, 12817 (2017).

[33]SØ Stub, K. Thorshaug, P. M. Rørvik, T. Norby, and E. Vøllestad, Phys. Chem. Chem. Phys. **20**, 15653 (2018).

[34]J. D. Baniecki, J. S. Cross, M. Tsukada, and J. Watanabe, Appl. Phys. Lett. **81**, 3837 (2002).

[35]M. D. Nguyen, C. T. Q. Nguyen, H. N. Vu, and G. Rijnders, J. Eur. Ceram. Soc. **38**, 95 (2018).

[36]D. M. Potrepka, M. Rivas, H. Yu, M. Aindow, G. R. Fox, and R. G. Polcawich, J. Mater. Sci. Mater. Electron. **29**, 11367 (2018).

[37]M. Carmo, D. L. Fritz, J. Mergel, and D. Stolten, Int. J. Hydrogen Energy **38**, 4901 (2013).

[38]T. S. Bjørheim, A. Kuwabara, I. Ahmed, R. Haugsrud, S. Stølen, and T. Norby, Solid State Ionics **181**, 130 (2010).

[39]H. Y. Huang, W. Y. Chu, Y. J. Su, J. X. Li, L. J. Qiao, and S. Q. Shi, Appl. Phys. Lett. **89**, 142904 (2006).

[40]M. Wu, H. Huang, W. Chu, L. Guo, L. Qiao, J. Xu, and T. Y. Zhang, J. Phys. Chem. C **114**, 9955 (2010).

[41]H. Y. Huang, W. Y. Chu, Y. J. Su, K. W. Gao, J. X. Li, and L. J. Qiao, J. Am. Ceram. Soc. **90**, 2062 (2007).

[42]L. W. Li, X. Sun, J. X. Li, L. J. Qiao, Y. J. Su, and W. Y. Chu, Appl. Surf. Sci. **255**, 7841 (2009).

[43]P. Bintachitt, P. Suaprasert, and P. Aungkavattana, Integr. Ferroelectr. **175**, 44 (2016).

[44]J. L. Cao, L. T. Li, Y. L. Wang, J. Q. Zhao, and Z. L. Gui, J. Mater. Sci. **37**, 3225 (2002).

[45]D. Zheng, J. Swingler, and P. Weaver, Sensors Actuators A Phys. **158**, 106 (2010).

[46]Y. Saito, T. Nakamura, K. Nada, and H. Sano, Jpn. J. Appl. Phys. **57**(11), 11UC04 (2018).

[47]M. Schalenbach, M. Carmo, D. L. Fritz, J. Mergel, and D. Stolten, Int. J. Hydrogen Energy **38**, 14921 (2013).

[48]M. Suermann, T. Kiupel, T. J. Schmidt, and F. N. Büchi, J. Electrochem. Soc. **164**, F1187 (2017).

[49]S. Brunauer, P. H. Emmett, and E. Teller, J. Am. Chem. Soc. **60**, 309 (1938).

[50]S. Barnartt, J. Electrochem. Soc. **106**, 722 (1959).

[51]H. N. Al-Shareef, K. D. Gifford, S. H. Rou, P. D. Hren, O. Auciello, and A. I. Kingon, Integr. Ferroelectr. **3**, 321 (1993).

[52]A. Okada, J. Appl. Phys. **48**, 2905 (1977).

[53]P. D. Thacher, Appl. Opt. **16**, 3210 (1977).

[54]R. H. T. Wilke, P. J. Moses, P. Jousse, C. Yeager, and S. Trolier-McKinstry, Sensors Actuators A Phys. **173**, 152 (2012).

[55]J. B. Quinn and G. D. Quinn, Dent. Mater. **26**, 135 (2010).

[56]D. Damjanovic, Rep. Prog. Phys **61**, 1267 (1998).

[57]A. Mazzalai, D. Balma, N. Chidambaram, P. Muralt, L. Colombo, and T. Schmitz-Kempen, in ISAF/IWATMD/PFM 2014 (IEEE, 2014), pp. 1–4.

[58]K. Coleman, J. Walker, T. Beechem, and S. Trolier-McKinstry, J. Appl. Phys. **126**, 034101 (2019).

[59]K. Coleman, R. Bermejo, D. Leguillon, and S. Trolier-McKinstry, Acta Mater. **191**, 245 (2020).

[60]S. W. Ko, W. Zhu, C. Fragkiadakis, T. Borman, K. Wang, P. Mardilovich, and S. Trolier-McKinstry, J. Am. Ceram. Soc. **102**, 1211 (2019).

[61]T. M. Borman, W. Zhu, K. Wang, S. W. Ko, P. Mardilovich, and S. E. Trolier-McKinstry, J. Am. Ceram. Soc. **100**, 3558 (2017).

[62]A. Warren, A. Nylund, and I. Olefjord, Int. J. Refract. Met. Hard Mater. **14**, 345 (1996).

[63]S. Kashiwaya, J. Morasch, V. Streibel, T. Toupance, W. Jaegermann, and A. Klein, Surfaces **1**, 73 (2018).

[64]S. Bagheri, N. A Muhd Julkapli, and S. Bee Abd Hamid, Sci. World J. **2014**, 727496 (2014).

[65]C. K. Huang, C. H. Chang, and T. B. Wu, J. Appl. Phys. **98**, 104105 (2005).

[66]W. P. Chen, Y. Wang, J. Y. Dai, S. G. Lu, X. X. Wang, P. F. Lee, H. L. W. Chan, and C. L. Choy, Appl. Phys. Lett. **84**, 103 (2004).

[67]A. Kiejna, in Encyclopedia on Interfacial Chemistry (Elsevier, 2018), pp. 319–326.

[68]J. Robertson and C. W. Chen, Mater. Res. Soc. Symp. Proc. **541**, 443 (1998).

[69]M. Grossmann, D. Bolten, O. Lohse, U. Boettger, R. Waser, and S. Tiedke, Appl. Phys. Lett. **77**, 1894 (2000).

[70]M. Grossmann, O. Lohse, T. Schneller, D. Bolten, U. Boettger, J. R. Contreras, H. Kohlstedt, and R. Waser, in Integrated Ferroelectrics (Taylor and Francis, 2001), pp. 205–214.

[71]M. Grossmann, O. Lohse, D. Bolten, U. Boettger, T. Schneller, and R. Waser, J. Appl. Phys. **92**, 2680 (2002).

[72]S. Stub, E. Vøllestad, and T. Norby, J. Mater. Chem. A **6**, 8265 (2018).

[73]I. A. Ryzhkin, M. I. Ryzhkin, A. M. Kashin, E. A. Galitskaya, and V. V. Sinitsyn, Europhys. Lett. **126**, 36003 (2019).

[74]Q. Li, Q. Yin, Y.-S. Zheng, Z.-J. Sui, X.-G. Zhou, D. Chen, and Y.-A. Zhu, J. Am. Chem. Soc. **35**, 9962 (2019).

[75]R. M. Pashley, M. Rzechowicz, L. R. Pashley, and M. J. Francis, J. Phys. Chem. B **109**, 1231 (2005).

[76]B. A. Boukamp, M. T. Pham, D. H. Blank, and H. J. Bouwmeester, Solid State Ionics **170**, 239 (2004).

[77]K. D. Kreuer, Solid State Ionics **125**, 285 (1999).

[78]J. M. Polfus, T. S. Bjørheim, T. Norby, and R. Bredesen, J. Mater. Chem. A **4**, 7437 (2016).

[79]V. I. Birss, J. Electrochem. Soc. **133**, 1621 (1986).

[80]S. P. Sharma and J. H. Thomas III, J. Vac. Sci. Technol. **14**, 825 (1977).

[81]S. Lee and R. W. Staehle, Mater. Corros. **48**, 86 (1997).

[82]C. T. Rueden, J. Schindelin, M. C. Hiner, B. E. DeZonia, A. E. Walter, E. T. Arena, and K. W. Eliceiri, BMC Bioinformatics **18**, 676 (2017).